Frequency Domain Unsteady Transonic Aerodynamics for Flutter and Limit Cycle Oscillation Prediction

Paulo C. Greco Jr.
pgreco@sc.usp.br
University of Sao Paulo
Engineering School of Sao Carlos
13566-590 Sao Carlos, SP, Brazil

Chuan-Tau E. Lan
vortex@ku.edu
University of Kansas
Aerospace Engineering Department
66045-7621 Lawrence, KS, USA

The purpose of this study was to develop new approaches for predicting transonic flutter and limit cycle oscillations (LCO) using computational methods. The TSD equation is separated into the in-phase and out-of-phase components through a nonlinear harmonic averaging method. It is then solved in the frequency domain to obtain the aerodynamic forcing function which is needed in the flutter and LCO analyses. To predict flutter, equations are developed using the concept of generalized coordinates. The flutter speed is determined by examining the frequency-domain matrix equation eigenvalues. Flutter characteristics of the AGARD I-445.6 wing are analyzed. Flutter speed and frequency are well predicted in subsonic speed, but are overestimated in supersonic flow. To predict limit cycle oscillations, the frequency-domain aerodynamic coefficients are used to obtain a nonlinear time-domain expression for the aerodynamic force. Limit cycle oscillation characteristics of the DAST ARW-2 wing are analyzed. The results show LCO for Mach numbers ranging from 0.915 to 0.940.
***Keywords**: aeroelasticity, transonic flow, frequency domain*

Introduction

Recent advances in Computational Fluid Dynamics (CFD) in conjunction with a large increase in computer processing speed raised interest in the study of unsteady transonic aerodynamics. The importance of estimating the aeroelastic characteristics in the transonic speed range has been known since World War II. At that time, tests with high-speed aircraft showed that the flutter dynamic pressure curve drops to a minimum in the transonic speed range, characterizing the so-called "transonic flutter dip". Limited available manpower, wind-tunnel resources, and increasing costs of testing time and models make experimental aeroelastic testing very expensive and time consuming. Flight tests are also needed to validate wind tunnel results. Theoretical solutions can reduce the cost of experimental testing by providing preliminary results for guidance.

A variety of fluid dynamics models is now available to address unsteady aerodynamic computations for aeroelastic applications. Methods that account for non-linear effects are being studied using the Full Potential equation (FPE), the Transonic Small Disturbance (TSD) equation, Euler equations (EE), Navier-Stokes equations (both Full (FNS) and Thin-Layer (TLNS)) or a combination of them. Edwards and Malone (1992) present a comprehensive review of computational methods for transonic unsteady aerodynamics.

One of the basic problems in transonic aerodynamics is that the flow is of mixed type with both subsonic and supersonic flows co-existing, and the location of the boundaries separating these flow regions is unknown. The real breakthrough came with the solution of the two-dimensional transonic small disturbance (TSD) equation by Murman and Cole (1971). Their important contribution is the development of a mixed-type finite difference scheme to solve the mixed (elliptic-hyperbolic) differential equation.

The XTRAN3S code was developed to solve the TSD equation using an alternating-direction implicit (ADI) finite-difference algorithm for treating simple 3-D cases. The employed method has a numerical stability restriction that requires a large number of sufficiently small time steps to obtain the solution (Cunningham, Batina and Bennett, 1988).

The CAP-TSD (Computational Aeroelasticity Program – Transonic Small Disturbance) solves the TSD equation in the time domain (Batina et al., 1987) using an approximate factorization (AF) solution algorithm which reduces or avoids the numerical stability restriction of the ADI algorithm used in the XTRAN3S code. Complete aircraft configurations can be analyzed.

Limit cycle oscillations typically occur in the transonic speed range where non-linear aerodynamic effects are more prominent. These non-linear effects make the theoretical prediction very difficult. Experimental prediction of LCO is also troublesome because, during tests, it is difficult to distinguish it from flutter. In addition, LCO occurs only within a narrow range of Mach numbers so that it is difficult to detect.

The role of shock-induced trailing-edge separation (SITES), as one of the inducing mechanisms in limit cycle oscillations, is discussed by Cunningham (1988). It is mentioned that strong interactions between shock and boundary layer may also induce LCO. A semi-empirical method for predicting LCO is described by Meijer and Cunningham (1991). In that investigation, the measured steady pressure distribution for a fighter configuration is used to identify non-linearities that could cause LCO. Again the focus is on the function of SITES on the development of limit cycle oscillations.

The aeroelastic characteristics of a supercritical wing were analyzed by Seidel et al. (1989). The wing was denoted DAST ARW-2 (Drones for Aerodynamic and Structural Testing – Aeroelastic Research Wing 2). Initial wind tunnel tests showed instabilities arising, in the transonic range, at a much lower dynamic pressure than the flutter boundary predicted using the doublet lattice theory. The motion was similar to the first bending mode. At a later date it was decided that the instability should be allowed to develop in the wind tunnel, past the point at which it was detected. In the initial tests this was avoided to prevent destruction of the model in case flutter occurred. The following tests showed that the instability was in fact limit cycle oscillations with maximum wing tip deflections occurring around Mach 0.9. This case illustrates the difficulties involved in identifying LCO and the importance of developing adequate theoretical prediction tools. An attempt to theoretically investigate this case was made by Bennett, Seidel and Sandford (1985) using the TSD code XTRAN3S. That attempt was unsuccessful and inaccuracies in predicting the steady flow field pressure distribution were mentioned as the probable cause.

In the present study, the TSD equation is solved in the frequency domain rather than in the time domain. To achieve this, the time-dependent TSD equation is first separated into the in-phase and out-of-phase components through a nonlinear harmonic averaging method. The equations then become similar in form to steady

Paper accepted March, 2010.Technical Editor: Eduardo Belo

aerodynamic equations, thus simplifying the problem. A computer code, developed at the University of Kansas under coordination of Dr. C. Edward Lan, is used to solve the unsteady TSD equation, in the frequency domain, for three dimensional aircraft configurations. That computer code was expanded and improved to analyze flutter and limit cycle oscillations.

Nomenclature

b_0 = *reference length, m*
c = *local chord, m*
g = *artificial structural damping ratio, dimensionless*
k = *reduced frequency, dimensionless*
m = *model mass, kg*
M = *local Mach number, dimensionless*
M_n = *generalized mass of the n^{th} mode, kg*
M_∞ = *free stream Mach number, dimensionless*
N = *number of structural normal modes, dimensionless*
q_∞ = *free stream dynamic pressure, Pa*
q_n = *generalized coordinate of the n^{th} mode, m*
$\overline{q}_n$ = *generalized coordinate amplitude of the n^{th} mode, m*
Q_n = *generalized force of the n^{th} mode, N*
$\overline{Q}_n$ = *generalized force amplitude of the n^{th} mode, N*
V_∞ = *free stream velocity, m/s*
V_f = *flutter speed, m/s*
z_n = *modal deflection of the n^{th} mode, m*

Greek Symbols

α_s = *steady state angle of attack, degrees*
γ = *ratio of specific heats, dimensionless*
δ = *phase angle between motion and aerodynamic response, degrees*
$\Delta\overline{p}$ = *differential lifting pressure amplitude, Pa*
θ = *instantaneous motion phase angle, degrees*
ρ = *air density, kg/m^3*
ϕ = *perturbation velocity potential, m^2/s*
ω = *frequency of oscillation, rad/s*
ω_0 = *reference frequency, rad/s*
ω_n = *natural frequency of the n^{th} mode, rad/s*

Theoretical Development

Unsteady Transonic Small Disturbance Equations in the Frequency Domain

A conservative-form, dimensionless, three-dimensional transonic small disturbance equation is derived from the full-potential equation:

$$(A\phi_t + B\phi_x)_t = (E\phi_x + F\phi_x^2 + G\phi_y^2)_x + (\phi_y + H\phi_x\phi_y)_y + (\phi_z)_z \tag{1}$$

where

$$A = M_\infty^2 k^2,\ B = 2M_\infty^2 k,\ E = 1 - M_\infty^2,\ F = -M_\infty^{1.75}(\gamma+1)/2,$$
$$G = M_\infty^2(\gamma-3)/2,\ H = M_\infty^2(1-\gamma),\ \mathrm{k} = \mathrm{b}_0\omega/V_\infty .$$

The equation is valid for unsteady, compressible, isentropic, irrotational flows. Corrections for entropy and vorticity effects are introduced through the use of modified coefficients (Batina, 1989). In the time-domain method, the TSD equation is directly integrated with small time steps. In the present approach the TSD equation is obtained in the frequency domain by using the method of harmonic averaging. The method of harmonic averaging has been used in the past to solve problems in nonlinear oscillations described by ordinary differential equations (Nayfeh and Mook, 1979). Hwang (1988) successfully applied it to compute the unsteady transonic flow about an airfoil by using the unsteady full-potential equation. It was shown that the main advantage of applying the averaging technique is to split a time-dependent equation into the in-phase and out-of-phase components which are similar in form to the steady flow equation. Therefore, the solution algorithm of steady flow equations can be directly adopted. In this way, time-domain integration of the unsteady flow equation can be avoided.

To apply this method, let the velocity potential be split into a steady and an unsteady component as

$$\phi(x,y,z,t) = \phi^{\mathrm{s}}(x,y,z) + \phi^{\mathrm{u}}(x,y,z)\cos(\theta+\delta) \tag{2}$$

where ϕ^s and ϕ^u are the perturbation velocity potentials for the steady and unsteady flow, respectively.

After the above expression is substituted into Eq. (1), the following steps are taken to perform the harmonic averaging:

1) Steady Flow: Dropping the unsteady terms in Eq. (1), the steady flow equation is obtained:

$$[\mathrm{E}\,\phi_x^{\mathrm{s}} + \mathrm{F}(\phi_x^{\mathrm{s}})^2 + \mathrm{G}(\phi_y^{\mathrm{s}})^2]_x + [\phi_y^{\mathrm{s}} + \mathrm{H}\,\phi_x^{\mathrm{s}}\phi_y^{\mathrm{s}}]_y + [\phi_z^{\mathrm{s}}]_z = 0 \tag{3}$$

2) Overall Averaging: Integrate Eq. (1) over one cycle and subtract the steady flow equation to obtain

$$[\mathrm{F}(\phi_x^{\mathrm{u}})^2 + \mathrm{G}(\phi_y^{\mathrm{u}})^2]_x + [\mathrm{H}\,\phi_x^{\mathrm{u}}\phi_y^{\mathrm{u}}]_y = 0 \tag{4}$$

3) In-Phase Averaging: Multiply Eq. (1) by $\cos\theta$ and then integrate it over one cycle to obtain

$$-\mathrm{A}\,\phi^{\mathrm{u(i)}} - \mathrm{B}\,\phi_x^{\mathrm{u(o)}} = [\mathrm{E}\,\phi_x^{\mathrm{u(i)}} + 2\,\mathrm{F}\,\phi_x^{\mathrm{s}}\phi_x^{\mathrm{u(i)}} + 2\,\mathrm{G}\,\phi_y^{\mathrm{s}}\phi_y^{\mathrm{u(i)}}]_x + [\phi_y^{\mathrm{u(i)}} + \mathrm{H}\,\phi_x^{\mathrm{s}}\phi_y^{\mathrm{u(i)}} + \mathrm{H}\,\phi_y^{\mathrm{s}}\phi_x^{\mathrm{u(i)}}]_y + [\phi_z^{\mathrm{u(i)}}]_z \tag{5}$$

where $\phi^{\mathrm{u(i)}} = \phi^{\mathrm{u}}\cos\delta$, $\phi^{\mathrm{u(o)}} = \phi^{\mathrm{u}}\sin\delta$.

4) Out-of-Phase Averaging: Multiply Eq. (1) by $\sin\theta$ and integrate it over one cycle to obtain

$$-\mathrm{A}\,\phi^{\mathrm{u(o)}} + \mathrm{B}\,\phi_x^{\mathrm{u(i)}} = [\mathrm{E}\,\phi_x^{\mathrm{u(o)}} + 2\,\mathrm{F}\,\phi_x^{\mathrm{s}}\phi_x^{\mathrm{u(o)}} + 2\,\mathrm{G}\,\phi_y^{\mathrm{s}}\phi_y^{\mathrm{u(o)}}]_x + [\phi_y^{\mathrm{u(o)}} + \mathrm{H}\,\phi_x^{\mathrm{s}}\phi_y^{\mathrm{u(o)}} + \mathrm{H}\,\phi_y^{\mathrm{s}}\phi_x^{\mathrm{u(o)}}]_y + [\phi_z^{\mathrm{u(o)}}]_z \tag{6}$$

5) In-Phase Equation: Multiply Eq. (4) by $\cos^2\delta$ and add Eq. (3) and Eq. (5) to obtain

$$-\mathrm{A}\,\phi^{\mathrm{u(i)}} - \mathrm{B}\,\phi_x^{\mathrm{u(o)}} = [\mathrm{E}\,\phi_x^{\mathrm{(i)}} + \mathrm{F}\,\phi_x^{\mathrm{(i)}2} + \mathrm{G}\,\phi_y^{\mathrm{(i)}2}]_x + [\phi_y^{\mathrm{(i)}} + \mathrm{H}\,\phi_x^{\mathrm{(i)}}\phi_y^{\mathrm{(i)}}]_z + [\phi_z^{\mathrm{(i)}}]_z \tag{7}$$

where $\phi^{\mathrm{(i)}} = \phi^s + \phi^{\mathrm{u(i)}}$.

6) Out-of-Phase Equation: Multiply Eq. (4) by $\sin^2\delta$ and add Eq. (3) and Eq. (6) to obtain

$$-\mathrm{A}\,\phi^{\mathrm{u(o)}} + \mathrm{B}\,\phi_x^{\mathrm{u(i)}} = [\mathrm{E}\,\phi_x^{\mathrm{(o)}} + \mathrm{F}\,\phi_x^{\mathrm{(o)}2} + \mathrm{G}\,\phi_y^{\mathrm{(o)}2}]_x + [\phi_y^{\mathrm{(o)}} + \mathrm{H}\,\phi_x^{\mathrm{(o)}}\phi_y^{\mathrm{(o)}}]_y + [\phi_z^{\mathrm{(o)}}]_z \tag{8}$$

where $\phi^{(o)} = \phi^s + \phi^{\mathrm{u}(o)}$.

Pressure Coefficients: The pressure coefficient is derived from Bernoulli's equation under the linear and small disturbance

assumptions, which neglect the perturbation velocities in y and z directions respectively (Dowell, 1978).

Wing Boundary Conditions: The wing boundary conditions are defined such that the normal velocity of the fluid at the wing surface equals the normal velocity on the wing.

Body Boundary Conditions: The body boundary conditions are satisfied not on the actual body surface. Instead, to simplify the grid interpolation, the body is replaced by a rectangular box. Even though the location of the body surface is changed, the original surface slope is preserved to obtain accurate aerodynamic loading.

Wake Boundary Condition: The wake boundary condition is defined such that the pressure difference across the wake vortex sheet is zero.

Far Field Boundary Conditions: The far field boundary conditions in supersonic flow field are derived by the method of characteristics to satisfy the non-reflecting properties from the far field boundaries (Hsu, 1994).

Finite Difference Equations

The governing equation has been decomposed into the in-phase and out-of-phase equations (Eq. (7) and Eq. (8)):

$$(E + 2F\phi_x^{(i)})\phi_{xx}^{(i)} + D\phi_y^{(i)}\phi_{xy}^{(i)} + (1 + H\phi_x^{(i)})\phi_{yy}^{(i)} + \phi_{zz}^{(i)} + A\phi^{u(i)} + B\phi_x^{(o)} = 0 \tag{9}$$

$$(E + 2F\phi_x^{(o)})\phi_{xx}^{(o)} + D\phi_y^{(o)}\phi_{xy}^{(o)} + (1 + H\phi_x^{(o)})\phi_{yy}^{(o)} + \phi_{zz}^{(o)} + A\phi^{u(o)} - B\phi_x^{(i)} = 0 \tag{10}$$

where

$$A = M_\infty^2 k^2,\ B = 2M_\infty^2 k,\ D = -2M_\infty^2 k,\ E = 1 - M_\infty^2,$$
$$F = -M_\infty^{1.75}(\gamma+1)/2,\ G = M_\infty^2(\gamma-3)/2,\ H = M_\infty^2(1-\gamma).$$

The partial derivatives of the velocity potentials are replaced by finite differences. The type-dependent differencing scheme proposed by Murman and Cole (1971) is applied. In the governing equation, the nonlinear coefficient of ϕ_{xx} will determine the flow regime after transforming Eq. (9) and Eq. (10) into a coordinate system aligning with the local flow (Sun, 1991). Central differencing is used if the coefficient is positive, which implies subsonic flow with an elliptic P.D.E., but upwind differencing is used for ϕ_{xx} if the coefficient is negative, implying supersonic flow with a hyperbolic P.D.E. An in-phase and an out-of-phase tridiagonal matrix equation in the k-direction are formed. Successive line over relaxation (SLOR) is used to solve the equations.

Surface Interpolation

The need for surface interpolation arises from the fact that the grid points necessary for the aerodynamic computations are not, in general, the same as those used in the structural modeling of the lifting surface. The method used for surface interpolation is described by Harder and Desmarais (1972).

Prediction Method for Transonic Flutter

The generalized structural equations of motion are obtained from Lagrange's Equations by expressing the airplane elastic deformation in terms of the structural normal (or natural) modes

$$z(x,y,t) = \sum_{n=1}^{N} z_n(x,y)\, q_n(t) \tag{11}$$

The generalized equations of motion are obtained as:

$$M_n \ddot{q}_n + M_n \omega_n^2 q_n = Q_n \quad , \quad n=1,2,...,N \tag{12}$$

Expressing the generalized coordinates and the generalized forces as

$$q_n = \bar{q}_n e^{i\omega t}$$
$$Q_n = \bar{Q}_n e^{i\omega t} \tag{13}$$

then Eq. (12) becomes

$$M_n(\omega_n^2 - \omega^2)\bar{q}_n = \bar{Q}_n \tag{14}$$

where the generalized force amplitude can be written as

$$\bar{Q}_n = \iint \Delta\bar{p}(x,y)\,dx\,dy \tag{15}$$

The lifting pressure amplitude is a function of the generalized coordinates

$$\Delta\bar{p} = \sum_{j=1}^{N} \Delta\bar{p}_j(x,y,\omega,M_\infty)\frac{\bar{q}_j}{b_0} \tag{16}$$

where $\bar{p}_j$ is the normalized lifting pressure amplitude of the j^{th} mode. Equation (15) then becomes

$$\bar{Q}_n = q_\infty b_0^2 \sum_{j=1}^{N}(a_{nj} + ib_{nj})\frac{\bar{q}_j}{b_0} \tag{17}$$

where

$$\begin{cases} a_{nj} = \iint \dfrac{\Delta\bar{p}_j^{(i)}}{q_\infty} z_n\, d\hat{x}\, d\hat{y} \\ b_{nj} = \iint \dfrac{\Delta\bar{p}_j^{(o)}}{q_\infty} z_n\, d\hat{x}\, d\hat{y} \end{cases}, \quad \begin{cases} \hat{x} = \dfrac{x}{b_0} \\ \hat{y} = \dfrac{y}{b_0} \end{cases} \tag{18}$$

The superscripts *i* and *o* indicate in-phase and out-of-phase respectively. By adding an artificial structural damping, *g*, in Eq. (14) results

$$M_n\left[\omega_n^2(1+ig) - \omega^2\right]\bar{q}_n = q_\infty b_0^2 \sum_{j=1}^{N}(a_{nj} + ib_{nj})\frac{\bar{q}_j}{b_0} \tag{19}$$

Eq. (19) can be rewritten in dimensionless form as

$$\sum_{j=1}^{N}(A_{nj} - \lambda\delta_{nj})\hat{q}_j = 0 \quad , \quad n = 1,2,...,N \tag{20}$$

where

$$A_{nj} = \left[\frac{\rho b_0^2}{2M_n}(a_{nj} + ib_{nj}) + k^2\delta_{nj}\right]\left(\frac{\omega_0}{\omega_n}\right)^2 \tag{21}$$

$$\lambda = \left(\frac{\omega_0 b_0}{V_\infty}\right)^2 (1+ig) \tag{22}$$

$$\hat{q}_j = \frac{\bar{q}_j}{b_0} \quad , \quad \delta_{nj} = \begin{cases} 0 \text{ if } n \neq j \\ 1 \text{ if } n = j \end{cases} \tag{23}$$

The eigenvalue problem is solved for λ and the damping ratio of each mode, *g*, is obtained from the imaginary part of each eigenvalue (Dowell, 1978). The quantity *g* indicates the amount of

structural damping required to make the system neutrally stable. The flutter speed corresponds to the minimum value of speed for which *g* is positive. Numerical interpolation was used to estimate the flutter speed, using a small number of reduced frequencies in solving the TSD equation, to save computing time. Eigenvalues were estimated using an eigenvalue extraction subroutine (Desmarais and Bennett, 1976).

Prediction Method for Limit Cycle Oscillations

For LCO prediction the aerodynamic force must be a nonlinear function of the elastic deformation. The total lifting pressure can be decomposed as

$$\Delta\bar{p} = \sum_{j=1}^{N} \Delta\bar{p}_j(x, y, k, \bar{q}, M_\infty) \tag{24}$$

Substituting Eq. (24) into Eq. (15) gives

$$\bar{Q}_n = \sum_{j=1}^{N} q_\infty \iint \Delta\bar{c}_{p_j} z_n \, dxdy \tag{25}$$

where

$$\Delta\bar{c}_{p_j} = \frac{\Delta\bar{p}_j}{q_\infty} \tag{26}$$

Rewrite Eq. (25) as

$$\bar{Q}_n = q_\infty b_0^2 \sum_{j=1}^{N} \bar{H}_{nj} \tag{27}$$

where

$$\bar{H}_{nj} = \iint \Delta\bar{c}_{p_j} z_n \, d\hat{x}d\hat{y} \quad , \quad \hat{x} = \frac{x}{b_0} \quad , \quad \hat{y} = \frac{y}{b_0} \tag{28}$$

The term $\bar{H}_{nj}$ is associated with the harmonic function

$$H_{nj} = \bar{H}_{nj} \, e^{i\Omega_j t} \tag{29}$$

where Ω_j is the instantaneous frequency of oscillation of the j^{th} mode. $\bar{H}_{nj}$ is assumed to be a function of reduced frequency and generalized coordinate amplitude as

$$\begin{aligned} \bar{H}_{nj} &= A_{nj}(k_j, \bar{q}_j) + i B_{nj}(k_j, \bar{q}_j) \quad \Rightarrow \\ H_{nj} &= \frac{A_{nj}(k_j, \bar{q}_j)}{\bar{q}_j} q_j + \frac{B_{nj}(k_j, \bar{q}_j)}{\bar{q}_j \Omega_j} \dot{q}_j \end{aligned} \tag{30}$$

From Eqs. (12), (27) and (30),

$$\ddot{q}_n + \omega_n^2 q_n = \frac{q_\infty b_0^2}{M_n} \sum_{j=1}^{N} \left[\frac{A_{nj}(k_j, \bar{q}_j)}{\bar{q}_j} q_j + \frac{B_{nj}(k_j, \bar{q}_j)}{\bar{q}_j \Omega_j} \dot{q}_j \right] \tag{31}$$

It is assumed that $A_{nj}/\bar{q}_j$ and $B_{nj}/\bar{q}_j$ can be expressed as the product of a linear function of reduced frequency with a linear function of generalized coordinate amplitude. This representation is arbitrarily chosen to give one of the simplest general polynomial representations which accounts for dependency on k_j and $\bar{q}_j$. Therefore, they can be written as

$$\begin{aligned} \frac{A_{nj}(k_j, \bar{q}_j)}{\bar{q}_j} &= (c_{1_{nj}} + c_{2_{nj}} k_j)(c_{3_{nj}} + c_{4_{nj}} \bar{q}_j) \\ &= e_{1_{nj}} + e_{2_{nj}} k_j + e_{3_{nj}} \bar{q}_j + e_{4_{nj}} k_j \bar{q}_j \\ \frac{B_{nj}(k_j, \bar{q}_j)}{\bar{q}_j} &= (d_{1_{nj}} + d_{2_{nj}} k_j)(d_{3_{nj}} + d_{4_{nj}} \bar{q}_j) \\ &= f_{1_{nj}} + f_{2_{nj}} k_j + f_{3_{nj}} \bar{q}_j + f_{4_{nj}} k_j \bar{q}_j \end{aligned} \tag{32}$$

The *e* and *f* coefficients are estimated, using least squares curve fitting, by obtaining $A_{nj}/\bar{q}_j$ and $B_{nj}/\bar{q}_j$ for several different values of reduced frequency, *k*, and generalized coordinate amplitude, $\bar{q}_j$. The least squares interpolation approximately fits the data to give the four *e* coefficients for the *A* function, and the four *f* coefficients for the *B* function.

Substitution of Eq. (32) into Eq. (31) produces

$$\begin{aligned} &\ddot{q}_n + \omega_n^2 q_n = \\ &\frac{q_\infty b_0^2}{M_n} \sum_{j=1}^{N} (e_{1_{nj}} + e_{2_{nj}} k_j + e_{3_{nj}} \bar{q}_j + e_{4_{nj}} k_j \bar{q}_j) q_j + \\ &\frac{q_\infty b_0^2}{M_n} \sum_{j=1}^{N} (f_{1_{nj}} + f_{2_{nj}} k_j + f_{3_{nj}} \bar{q}_j + f_{4_{nj}} k_j \bar{q}) \frac{\dot{q}_j}{\Omega_j} \end{aligned} \tag{33}$$

In Eq. (33) the generalized force is a non-linear function of the generalized coordinate and is valid for an oscillatory motion. That equation can be integrated in time from an initial disturbance (initial value problem).

Then the stability of the system can be examined from the obtained time history in the generalized coordinate. From Eq. (11) it can be seen that the resulting displacement time history for any point on the structure is given by the summation of the generalized coordinate time histories multiplied by the corresponding normal mode deflections.

Time Integration of Flutter Equations

The nonlinear flutter equations were integrated in time using the automatic multi-dimensional Runge-Kutta-Fehlberg program RKF45 described by Atkinson (1988).

Effect of Shock-Boundary Layer Interaction

The computer code was modified to use the method described by Lee (1990) to model the effect of shock induced flow separation. The effect of a suddenly thickened boundary layer behind a shock is treated as an equivalent vertical surface velocity.

Results and Discussion

A computer code was developed at the University of Kansas, under coordination of Dr. C. Edward Lan, to solve the unsteady TSD equation in the frequency domain using the method described in the present study. That computer code was named USTSD (UnSteady Transonic Small Disturbance).

The USTSD code was validated for predicting unsteady pressure distributions in a study by Hsu (1994). In the present study, the original USTSD code was expanded and improved to include the capability of predicting transonic flutter and LCO.

Flutter Estimation

The AGARD I-Wing 445.6: This test case is generally used as a standard for validating methods of flutter estimation (Yates, Land and Foughner, 1963). It consists of a cantilevered wing with a half-span aspect ratio of 1.65, taper ratio of 0.66, quarter-chord

sweepback angle of 45° and NACA 65A004 airfoil section in the stream wise direction.

Weakened model 3 has a wing span of 0.76 m, a root chord of 0.56 m, and the structure was made more flexible by drilling holes through the wing and filling with foam plastic to maintain aerodynamic continuity. Five wing normal modes were obtained along with the corresponding natural frequencies and generalized masses. The flutter results are presented in Fig. 1.

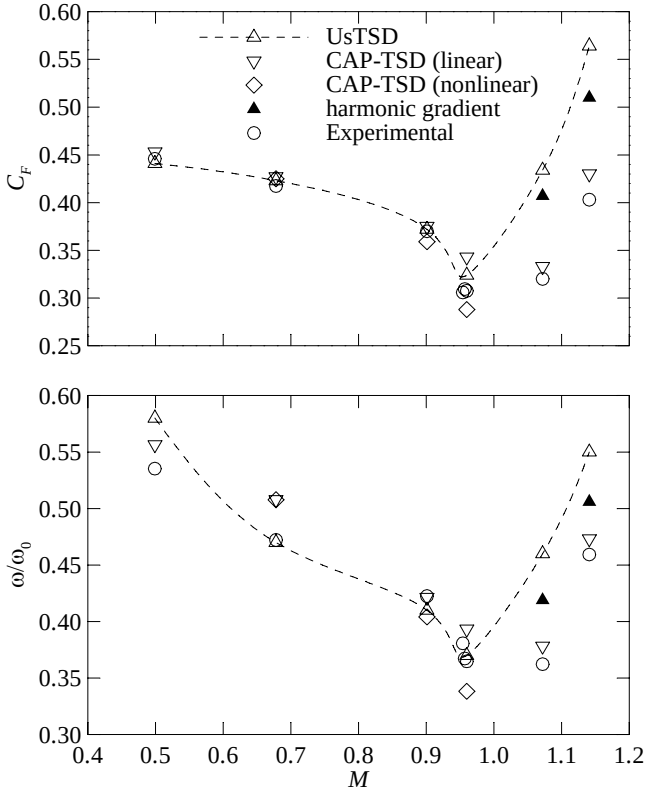

Figure 1. Flutter speed index and frequency ratio curves for the I–Wing 445.6 weakened model 3.

The flutter speed index, C_F, is defined as

$$C_F = \frac{V_f}{b_0 \omega_0 \sqrt{\mu}} \tag{34}$$

where the mass-density ratio, μ, is given by

$$\mu = \frac{m}{\rho \upsilon} \tag{35}$$

where υ is the volume of a conical frustum having wing chord at root as base diameter, wing tip chord as upper diameter and wing semi-span as height.

The CAP-TSD estimations (Cunningham, Batina and Bennett, 1988) include both linear and non-linear results. The linear results were obtained by setting coefficients F, G and H equal to zero in the TSD equation (Eq. (1)) and by neglecting wing thickness.

It is interesting to notice that, in the subsonic range, the linear estimations show a good agreement with the experimental results, except at Mach 0.96 where non-linear effects are expected to play a major role. This good agreement might be justified by the fact that the model has a very thin airfoil section, so wing thickness can be neglected. In the supersonic range the linear results show higher flutter speed indices than the experimental values. This appears to be a general trend and is also observed in an aeroelastic analysis of the F-15 wing (Pitt and Fuglsang, 1992), in which CAP-TSD was used. The reasons for this trend are not clear and require further investigation. The non-linear estimations are limited to three points at Mach 0.678, 0.901, and 0.96 and show, as expected, a slightly better result at Mach 0.96 compared to the linear estimation.

The harmonic gradient results were obtained from a study by Wong, Lee and Murty (1992). Only the two points in the supersonic range at Mach 1.072 and 1.141 were included, to show the consistently higher values for the flutter speed index obtained in that range. The harmonic gradient method is described by Chen and Liu (1985).

The USTSD results for the flutter speed index show good agreement with the experimental data except in the supersonic range for which the flutter speed indices are higher than the experimental values. The transonic dip is shown very clearly around Mach 1.0. The flutter frequency ratio results from USTSD agree well with the experimental results except, again, for supersonic speeds.

Limit Cycle Oscillations

Characteristics of the DAST ARW-2 Wing: The DAST ARW-2 (Drones for Aerodynamic and Structural Testing Aeroelastic Research Wing 2) is a supercritical wing with aspect ratio of 10.3 and leading edge sweep angle of 28.8 degrees. The stream wise wing sections are defined by three supercritical airfoils described in a study by Eckstrom, Seidel and Sandford (1994) at spanwise locations 7.1%, 42.6% and 100%. Five wing normal modes were obtained (Sandford, Seidel and Eckstrom, 1989).

ARW-2 Wing LCO Prediction Using USTSD Code: In this present study an attempt was made to predict the ARW-2 limit cycle oscillations. The following conditions are chosen for the study:

1) ARW-2 wing alone configuration;
2) Control surfaces are not deflected;
3) Zero angle of attack;
4) Air medium (standard atmosphere);
5) Mach number ranging from 0.8 to 0.95 with corresponding dynamic pressure range from 6,000 to 8,000 Pa (altitude of about 15,000 m).

For the initial calculations fully conservative finite difference scheme, with shock/boundary-layer interaction correction, was used. The results showed instability at Mach 0.92, but limit cycle was not achieved. The correct trend was observed, with the system becoming less unstable as the amplitude grows. However, the system remained unstable for what was considered a reasonable range of amplitude (keeping in mind the small disturbance assumption). Following calculations using non-conservative differencing and no shock-boundary layer interaction produced the correct trend for the instability, becoming stable for a reasonable value of amplitude. It is known that the use of non-conservative differencing in some cases produces results that are closer to experimental results than using conservative differencing (Anderson, Tannehill and Pletcher, 1981).

A case study with prominent shock-boundary layer interaction was investigated to validate the use of non-conservative differencing in such problems. That case study is the RAE 2822 airfoil at Mach 0.73 (Lee, 1990). As Fig. 2 shows, the results obtained using the USTSD computer code with non-conservative differencing are closer to the experimental results than the other results, specifically on the upper surface where the shock is located. This indicates that non-conservative differencing may be more accurate for cases where shock/boundary-layer interaction is important.

Once it was decided that the use of non-conservative differencing was justified with the ARW-2 wing, an investigation of the relative importance of each normal mode on the instability was conducted.

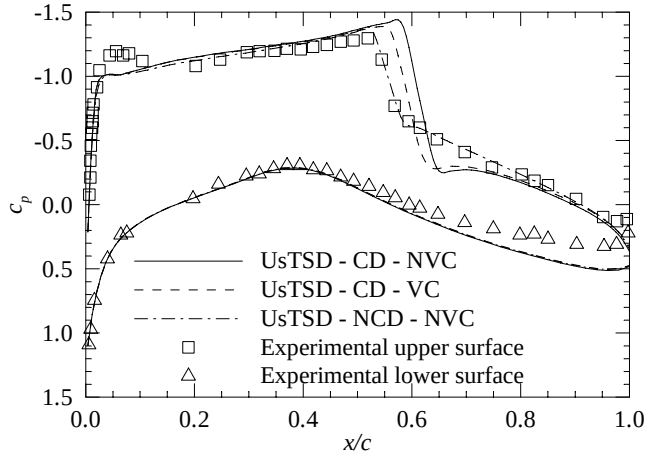

Figure 2. Steady pressure distribution for the RAE 2822 airfoil at *M* = 0.73 and α = 3.19°. CD: conservative differencing, NCD: non-conservative differencing, VC: with viscous correction, NVC: no viscous correction.

The ARW-2 aeroelastic characteristics were obtained using the flutter prediction method with the following conditions:

1) Mach 0.92;
2) Dynamic pressure of 7300 Pa;
3) Altitude of 15,000 m (standard atmosphere);
4) Reduced frequency of 0.105;
5) Reference length of 0.562 m.

Flutter analysis results were obtained using only the first normal mode and using all five normal modes. One eigenvalue is obtained when only the first normal mode is considered. Five eigenvalues are obtained when all five normal modes are considered. Each eigenvalue has a corresponding value of airspeed, frequency and damping required for neutral stability (Eq. (22)). Only the first eigenvalue had airspeed compatible with the specified Mach number and altitude. The other eigenvalues had airspeeds too high for the assumed Mach number and altitude. Therefore, only the first eigenvalue should be considered in the aeroelastic analysis at that particular Mach number and altitude. Examination of the results for the first eigenvalue showed that they do not change significantly if just one or all five modes are considered. The eigenvector corresponding to the first eigenvalue showed that the first mode had a relative contribution to the elastic deformation over 100 times larger than that of the other modes. Based on those results, only the first bending mode was considered in the analysis of the ARW-2 instability. This assumption is consistent with the experimental results that showed that the ARW-2 limit cycle oscillations had characteristics similar to the first bending mode.

The first prediction of the ARW-2 limit cycle oscillations was carried out at the following conditions:

1) Mach 0.92;
2) Dynamic pressure of 7300 Pa;
3) Altitude of 15,000 m (standard atmosphere);
4) Reduced frequencies of 0.115, 0.110, 0.105, 0.100, 0.095;
5) Amplitudes of generalized coordinate of 0.02, 0.06, 0.12, 0.18, 0.24 m;
6) Reference length of 0.562 m;
7) Initial displacement for generalized coordinate of 3 mm for the time integration (initial disturbance).

The generalized aerodynamic force (GAF) coefficients a_{nj} and b_{nj} (Equation (18)) were obtained using program USTSD with the conditions described above. Figure 3 shows the out-of-phase GAF coefficients as a function of the reduced frequency and amplitude of generalized coordinate.

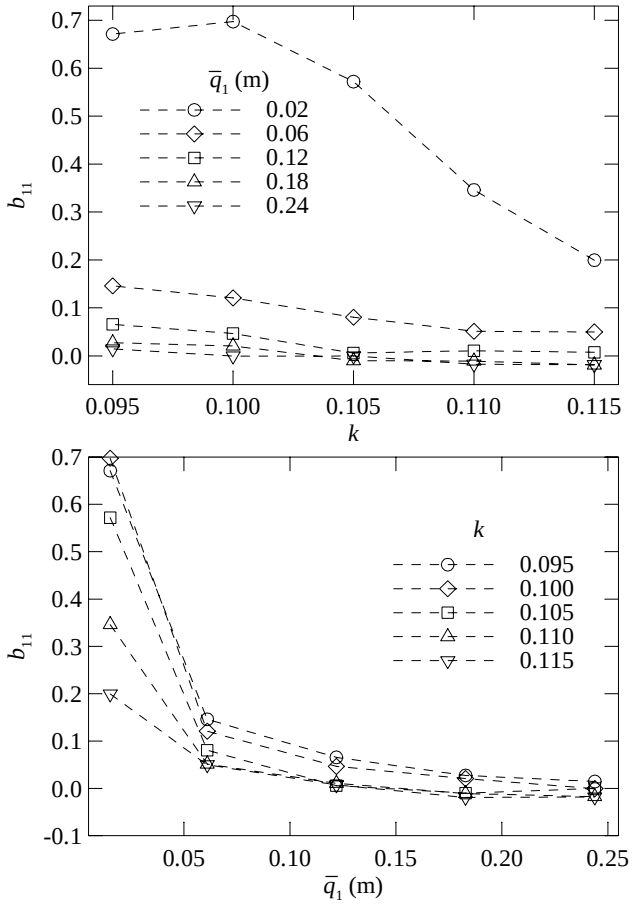

Figure 3. Out-of-phase GAF coefficient for the ARW-2 wing at *M* = 0.92, α = 0° and b_0 = 0.562 m.

The sign of the out-of-phase GAF coefficient indicates whether the system is stable or not, for a single degree-of-freedom case. The system is stable if the coefficient is negative and unstable if it is positive.

Figure 3 shows that, for a fixed value of amplitude, the system becomes more unstable as the reduced frequency is decreased. This is equivalent to saying that, for a given frequency of oscillation, the system becomes more unstable as the airspeed is increased. This is consistent with the physical phenomena of flutter and LCO: the system is stable at low speeds, but becomes unstable as the speed is increased. Also, from Fig. 3 it can be seen that, for a fixed value of reduced frequency, the system becomes asymptotically more stable as the amplitude of generalized coordinate is increased. This is consistent with LCO: the system is unstable for small amplitudes of oscillation, but becomes stable as the amplitude increases.

To explain the trends observed in Fig. 3 the pressure distribution was analyzed. Figure 4 shows the out-of-phase unsteady pressure coefficient distribution at 80%, 87% and 95% spanwise sections, at Mach 0.92, obtained using non-conservative differencing.

The wing region close to the tip was chosen for analysis because that is where the largest elastic deformations occur for the first bending mode. The larger the deflection is, in a region of the structure, the greater the contribution of that region to the GAF

coefficient is (see Eq. (18)). The out-of-phase pressure distribution defines the out-of-phase generalized aerodynamic force and, therefore, defines whether the system is stable or not. It can be seen that there is a differential pressure peak near the locations of the steady pressure shock. Positive values of the out-of-phase differential pressures are in phase with the first bending mode velocity and have a destabilizing effect (positive work). Negative values of out-of-phase differential pressures are 180° out of phase with respect to the first bending mode velocity and have a stabilizing effect (negative work).

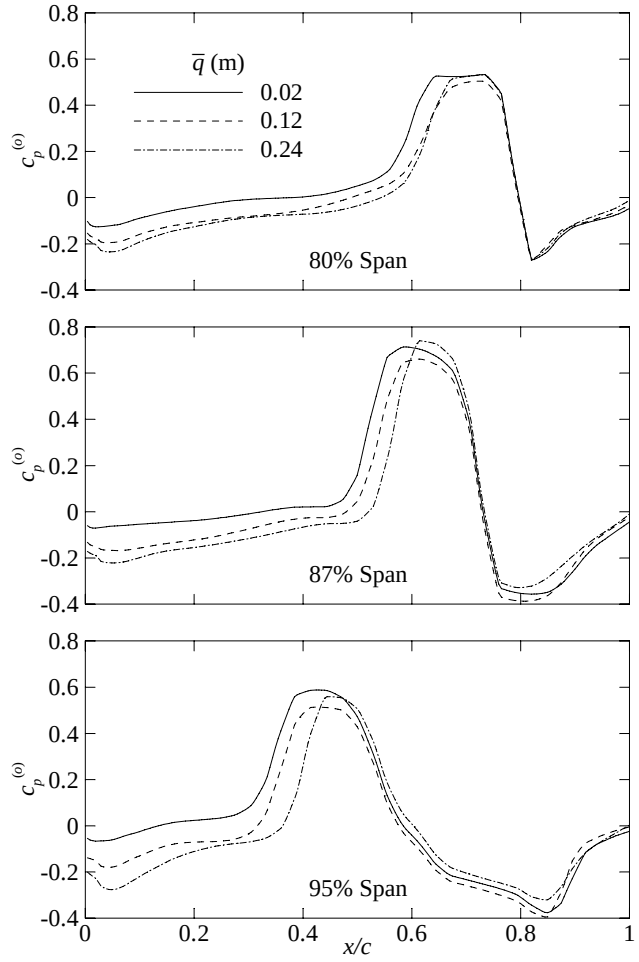

Figure 4. Out-of-phase unsteady differential pressure coefficient for the ARW-2 wing at M = 0.92, α = 0° and b_0 = 0.562 m using non-conservative differencing.

It can be seen in Fig. 4 that the area of the positive differential pressure peaks is reduced as the amplitude of generalized force coordinate is increased. Also, the area of the negative differential pressure near the leading edge is increased as the amplitude of generalized force coordinate is increased. Both trends cause the system to become more stable as the amplitude of oscillation increases, characterizing limit cycle oscillations. The two causes for LCO for this particular example seem to stem from a very mild reduction in shock strength as the amplitude of oscillation increases in conjunction with changes in the pressure distribution around the leading edge. The aerodynamic undamping that starts LCO at small amplitudes is usually very small and the changes in pressure distribution that occur as amplitude increases do not have to be strong to drive the system to a stable condition.

The generalized equations of motion were obtained using the method for LCO prediction and integrated in time using the Runge-Kutta-Fehlberg method. The time history for displacement, instantaneous amplitude and frequency at Mach 0.92 is shown in Fig. 5. The results show limit cycle oscillations with the maximum amplitude of about 10 centimeters and frequency of about 8.1 Hz. The amplitude is higher than the experimental result of 5 cm and the frequency is lower than the experimental result of about 9 Hz. The wing first bending mode has a natural frequency of 8.1 Hz which shows that frequency matching is associated with the occurrence of LCO.

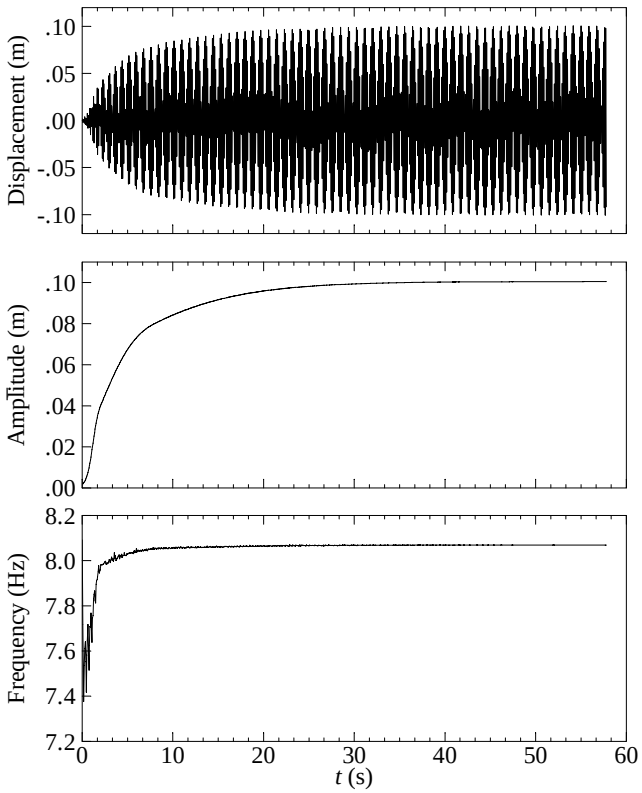

Figure 5. Time history for the ARW-2 wing at M = 0.92, α_s = 0°, b_0 = 0.562 m, q_∞ = 7300 Pa and altitude of 15,000 m.

LCO was observed for Mach numbers between 0.915 and 0.940. All results are plotted in Fig. 6 along with the experimental results. The experimental results show LCO for a wide range of Mach numbers with the maximum occurring around Mach 0.93. Usually, LCO is expected to occur for a narrow range of Mach numbers. One possible reason for the large differences between estimated and experimental results is that not enough nonlinear aerodynamic damping terms (the f coefficients of Eq. (33)) were considered in the calculation. It is expected that including terms of higher degree would improve data fitting for the B function and, thus, increase the accuracy of the prediction. The calculated results show LCO for a Mach number range from 0.915 to 0.94 and the maximum occurs around Mach 0.94.

Conclusions

The method described in the present study for predicting flutter produced good results, when compared to experimental results, in the subsonic and transonic speed ranges, for the AGARD I-445.6 wing. For the supersonic range the computed flutter results were significantly different from the experimental results. This difference was consistent with published data obtained using the harmonic gradient method. The method used in this study to predict limit cycle

oscillations showed LCO for the DAST ARW-2 wing in Mach numbers ranging from 0.915 to 0.94. The Mach number range at which LCO occurred was much narrower than the experimental. The calculated maximum amplitudes were about 2 to 3 times larger than the experimental results. For both experimental and calculated results the largest value of maximum amplitude occurred around Mach 0.93.

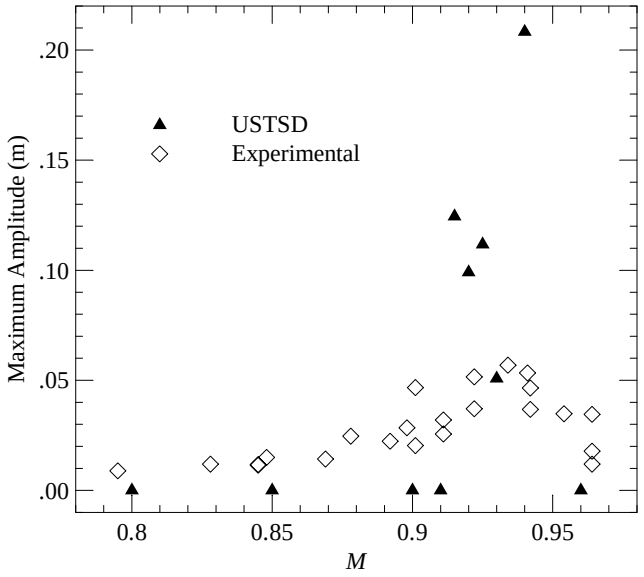

Figure 6. Maximum deflections for the ARW-2 wing at $\alpha_s = 0^o$, $b_0 = 0.562$ m, $q_\infty = 7300$ Pa and altitude of 15,000 m.

The use of non-conservative differencing produced better results than the use of conservative differencing with corrections for shock/boundary-layer interaction. Study of a RAE airfoil showed that, in some cases, the use of non-conservative differencing may produce good results for the shock/boundary-layer interaction effect. This effect was produced by moving the shock upstream and reducing its strength.

The mechanism that caused LCO in the case studied seems to be a combination of weakening of upper surface shock and changes in leading edge pressure distribution as the amplitude of oscillation increases.

The higher frequency normal modes could have and important effect on the flutter speed and frequency, in the supersonic range, for the AGARD I-445.6 wing. Inaccuracies in obtaining the structural normal modes could also have significant impact on the results.

Even though the use of non-conservative differencing produced reasonable results for shock-wave/boundary-layer interaction, it is unknown if this approach would work for other test cases. It would be preferable to find an effective method to correct for viscous effects without compromising the conservative properties.

The LCO characteristics of the ARW-2 wing were obtained considering only the first bending mode. The validity of the single-degree-of-freedom assumption was not verified by comparing the results when all five normal modes are included in the calculation. The effect of factors like steady state angle of attack, control surface deflection and test medium on LCO characteristics was not investigated.

The LCO results presented are just an indication that the method used in this study works. It would be necessary to explore more cases before the method is validated. The main obstacle to achieving that objective is that it is currently very difficult to obtain complete LCO experimental data. Such data would have to consist of not only aerodynamic data, but also a very good description of the structural properties.

References

Anderson, D.A., Tannehill, J.C. and Pletcher, R.H., 1984, "Computational Fluid Mechanics and Heat Transfer", Hemisphere Publishing Corporation, 52 p.

Atkinson, K.E., 1988, "An Introduction to Numerical Analysis", Second Edition, John Wiley & Sons.

Batina, J., 1989, "Unsteady Transonic Small-Disturbance Theory Including Entropy and Vorticity Effects", *Journal of Aircraft*, Vol. 26, No. 6, pp. 531-538.

Batina, J.T., Seidel, D.A., Bland, S.R. and Bennett, R.M., 1989, "Unsteady Transonic Flow Calculations for Realistic Aircraft Configurations", *Journal of Aircraft*, Vol. 26, No. 1, January 1989, pp. 21-28 (Also NASA TM-89120, March 1987).

Bennett, R.M., Seidel, D.A. and Sandford, M.C., 1985, "Transonic Calculations for a Flexible Supercritical Wing and Comparisons with Experiment", AIAA Paper 85-0665-CP, April.

Chen, P.C. and Liu, D.D., 1985, "A Harmonic Gradient Method for Unsteady Supersonic Flow Calculations", *Journal of Aircraft*, Vol. 22, May 1985, pp. 371-379.

Cunningham, Jr., A.M., 1988, "Practical Problems: Airplanes", in Unsteady Transonic Aerodynamics, Progress in Astronautics and Aeronautics, Vol. 120, Chapter 3, edited by Nixon, D.

Cunningham, H.J., Batina, J.T. and Bennett, R.M., 1988, "Modern Wing Flutter Analysis by Computational Fluid Dynamics Methods", NASA TM-100531, January.

Desmarais, R.N. and Bennett, R.M., User's Guide for a Parametric Flutter Eigenvalue Program, June 1976.

Dowell, E.H., "A Modern Course in Aeroelasticity", Sijthoff & Noordhoff, Maryland, 1978.

Eckstrom, C.V., Seidel, D.A. and Sandford, M.C., 1994, "Measurements of Unsteady Pressure and Structural Response for an Elastic Supercritical Wing", NASA Technical Paper 3443, November.

Edwards, J.W. and Malone, J.B., 1992, "Current Status of Computational Methods for Transonic Unsteady Aerodynamics and Aeroelastic Applications", AGARD-CP-507, March.

Harder, R.L., and Desmarais, R.N., 1972, "Interpolation Using Surface Splines", *Journal of Aircraft*, Vol. 9, No. 2, February.

Hsu, C., 1994, "Calculation of Unsteady Pressure Distributions and Dynamic Stability Parameters by an Unsteady Transonic Small-Disturbance Theory in Frequency Domain", M.S. Thesis, The University of Kansas.

Hwang, H., 1988, "Computation of Unsteady Transonic Flow About Airfoils in Frequency Domain Using the Full-Potential Equation", Ph.D. Dissertation, The University of Kansas.

Lee, S.C., 1990, "A Fast Viscous Correction Method for Transonic Aerodynamics", Computational Methods in Viscous Aerodynamics, Chapter 10, T.K.S. Murthy and C. A. Brebbia, Elsevier, N.Y.

Meijer, J.J. and Cunningham, A.M., Jr., 1991, "Development of a Method to Predict Transonic Limit Cycle Oscillation Characteristics of Fighter Aircraft", AGARD-CP-507.

Murman, E.M. and Cole, J.D., 1971, "Calculation of Plane Steady Transonic Flows", *AIAA Journal*, Vol. 9, January, pp. 114-121.

Nayfeh, A.H. and Mook, D.T., 1979, "Nonlinear Oscillations", John Wiley & Sons Publication.

Pitt, D.M. and Fuglsang, D.F., 1992, "Aeroelastic Calculations for Fighter Aircraft Using the Transonic Small Disturbance Equation", AGARD-CP-507, March.

Sandford, M.C., Seidel, D.A. and Eckstrom, C.V., 1989, "Geometrical and Structural Properties of an Aeroelastic Research Wing (ARW-2)", NASA TM-4110.

Seidel, D.A., Eckstrom, C.V. and Sandford, M.C., 1989, "Transonic Region of High Dynamic Response Encountered on an Elastic Supercritical Wing", *Journal of Aircraft*, Vol. 26, No. 9, September, pp. 870-875.

Sun, T.H., 1991, "Unsteady Transonic Aerodynamics in Frequency Domain for Flutter Analysis", Ph.D. Dissertation, The University of Kansas.

Wong, Y.S., Lee, B.H.K. and Murty, H.S., 1992, "A Time-Linearization Approach for Unsteady Transonic Flows", AGARD CP-507.

Yates, E.C., Jr., Land, N.S. and Foughner, J.T., Jr., 1963, "Measured and Calculated Subsonic and Transonic Flutter Characteristics of a 45^o Sweptback Wing Planform in Air and in Freon-12 in the Langley Transonic Dynamics Tunnel", NASA TN D-1616.